The Astrophysical Journal, 728:69 (11pp), 2011 February 10 doi:10.1088/0004-637X/728/1/69

THE SURFACE OF V410 TAURI

J. B. Rice[1,2,3], K. G. Strassmeier[2], and M. Kopf[2]
[1] Department of Physics, Brandon University, Brandon, Manitoba R7A 6A9, Canada; rice@BrandonU.ca
[2] Astrophysical Institute Potsdam, An der Sternwarte 16, D-14482 Potsdam, Germany; KStrassmeier@aip.de, mkopf@aip.de
Received 2010 July 11; accepted 2010 November 17; published 2011 January 21

ABSTRACT

We present Doppler images of the weak-lined T Tauri star V410 Tau obtained with two different Doppler-imaging codes. The images are consistent and show a cool extended spot, symmetric about the pole, at a temperature approximately 750 K below the average photospheric value. Smaller cool spots are found fairly uniformly distributed at latitudes below the polar cap with temperatures about 450 K below the average photospheric temperature. Resolution on the stellar surface is limited to about 7° of arc, so structure within these spots is not visible. Also at lower latitudes are hotter features with temperatures up to 1000 K above the photosphere. A trial Doppler image using a TiO molecular feature reproduced the cool polar cap at a temperature about 100 K below the value from the atomic line images. The equatorial features, however, were not properly reproduced since Doppler imaging relies on information in the wings of lines for reconstructing equatorial features, and for V410 Tau these molecular band lines overlap. In 1993, V410 Tau had a large photometric amplitude resulting from the concentration of cool spots on the hemisphere of the star visible at phase 0°, a phenomenon known as preferred longitude. In contrast, the small photometric amplitude observed currently is due to a strong symmetric polar spot and the uniform distribution in longitude of equatorial cool and warm spots. This redistribution of surface features may be the beginning of a slow "flip-flop" for V410 Tau where spot locations alternate between preferred longitudes. Flare events linked to two of the hotter spots in the Doppler image were observed.

Key words: stars: imaging – stars: individual (V410 Tau) – starspots

Online-only material: machine-readable table, color figure

1. INTRODUCTION

Cool spots on the surfaces of stars are now the standard explanation for the sometimes large, sometimes subtle, light variations of late-type stars (see reviews by Berdyugina 2005 and Strassmeier 2009 and many references therein). Starspots also turned out to be a serious physical limit for the detection of extrasolar planets, in particular of (super-)Earth size and smaller, either via the radial-velocity method (Hatzes 2002) or the transit method (Alapini & Aigrain 2009).

Light variations due to starspots are always modulated with the rotation period of the star at that particular latitude where the spot occurs (Hall 1972). Modeling of multiple cycles of a light curve with more than one spot at different latitudes allows us to make an order-of-magnitude determination of surface differential rotation, one of the main ingredients of a stellar dynamo. However, light curves cannot reveal the sign of differential rotation, i.e., to decide whether the polar regions rotate faster or slower than the equatorial regions, which is of great importance for a dynamo model (see Kitchatinov & Rüdiger 2005). One needs Doppler images from a series of high-resolution spectral line profiles to do so. This technique, sometimes also referred to as Doppler tomography, allows us to reconstruct the surface temperature or brightness distribution from periodic variations of spectral line profiles (e.g., Rice 2002).

There is yet another important reason, in addition to differential rotation, why we need disk-resolved information of spotted stellar surfaces. Light curves, even if multi-color, cannot be modeled with a mathematically unique solution. The simple reason is that a light curve in a particular bandpass can be equally well described with a cool spot and a slightly warmer photosphere as with a warm spot and a slightly cooler photosphere. Multi-bandpass light curves can constrain this problem somewhat (if the wavelength dependent limb darkening/brightening is properly taken into account), but still cannot exclude the coexistence of smaller hot spots. There is a number of active stars where the "blue" color indices, such as $U-B$ and $B-V$, vary in antiphase with the "red" color indices, usually $V-I$ (e.g., Aarum Ulvas & Engvold 2003; Frasca et al. 2008). The most likely explanation is that hot plages accompany cool spots, as on the Sun. This geometry is fatal for the modeling of integrated band light curves from current photometric space telescopes because their "filter bandpass" spans almost the entire optical wavelength range and delivers a mixed phenomenon light curve. Fortunately, Doppler imaging (DI) can resolve this as well. It only requires that the line-profile inversion preserves the temperature information, which is achieved with a full radiative transfer approach for the computation of the local line profile (Piskunov & Rice 1993; Rice 2002; Carroll et al. 2007).

Another starspot-related phenomenon is that of active longitudes. For many stars, stellar activity is dominated by long-lived complexes of spots at preferred longitudes for periods of time that exceed the lifetimes of individual spots. These longitudes of ongoing excesses of spot activity are called active longitudes. Active longitudes were detected on many active stars, binaries as well as single stars (e.g., Korhonen et al. 2001; Oláh et al. 2002; Berdyugina et al. 2002; Oláh 2006; Järvinen et al. 2005), and are explained with a dynamo-related phenomenon (Elstner & Korhonen 2005). Long-term photometric observations of weak-lined T Tauri stars (WTTS) revealed the same phenomenology as for some of the most active RS CVn binaries and FK Comae

[3] Based on observations obtained at the Canada–France–Hawaii Telescope (CFHT) which is operated by the National Research Council of Canada, the Institut National des Sciences de l'Univers of the Centre National de la Recherche Scientifique of France, and the University of Hawaii.

stars (e.g., Vrba 1988; Herbst 1989). Just recently, Grankin et al. (2008) suggested the existence of active longitudes on several WTTS on the basis of stable photometric minima and noted that the phenomenon is most pronounced in V410 Tau. Its change in the phase of the light curve minimum did not vary by more than 0.16 rotation periods over the course of 19 years.

In some stars, the longitude of the predominant activity region on the stellar surface switches quasi-periodically by 180°, a behavior known as the "flip-flop" phenomenon (Korhonen et al. 2001).

In this paper, we present a new Doppler image of V410 Tau from 2008/2009. We employ our two DI codes TempMap and iMAP, the former with a direct multiple line approach and the latter with a principal component analysis (PCA)-based signal de-noising approach (Martínez González et al. 2008). Additionally, TempMap is used with the TiO molecular band. There are now comparisons that can be made with previous images of V410 Tau that allow us to see the time development of the active regions. We also present our long-term automatic photometry of V410 Tau, now covering 13 consecutive years. The long-term goal of this research is to identify the contrasts in behavior for all active stars with the behavior of the Sun.

A later paper will deal with Zeeman–Doppler imaging (ZDI) of V410 Tau to extract the magnetic field distribution and orientation based on the Stokes V observations from the current data set and the temperature mapping reported in this paper.

2. OBSERVATIONS AND INVERSION SOFTWARE

2.1. CFHT Spectroscopy in 2008/09

High-resolution spectroscopic observations were obtained with the ESPADONS echelle spectrograph and polarimeter (Donati et al. 1998) in Stokes I and V at the 3.6 m CFHT on Mauna Kea, Hawaii. Data were obtained in queue mode during one observing block over four nights from 2008 October 15 to 19, and one over 13 nights distributed between the dates of 2008 December 5 to 2009 January 14. A spectral resolution of 60,000 with a useful wavelength coverage of 390–900 nm was obtained. All integrations on V410 Tau ($V \approx 11\overset{\mathrm{m}}{.}0$) were set to an exposure time of 4 × 600 s. This allowed for a total of 17 spectra with an average signal-to-noise (S/N) ratio of around 160:1 per single exposure per pixel.

All spectra were reduced and extracted using the Libre–ESPRIT package provided by CFHT and executed automatically. Details of this reduction procedure are given in Donati et al. (1997).

2.2. APT Photometry from 1996 to 2009

Photoelectric photometry of V410 Tau was obtained with the University of Vienna 0.75 m twin automatic photoelectric telescopes (APTs) at the Fairborn Observatory in southern Arizona (Strassmeier et al. 1997). The T7-APT used Johnson–Cousins VI_C filters and observed from JD 2,450,395 in 1996 through 2,454,892 in 2009 on every clear night (and still ongoing). It initially achieved an external precision of 5 mmag in V that degraded to 20 mmag in late 2008 due to a defect in the positioning CCD camera that prevented determining how badly the telescope was out of focus. Unfortunately, this camera had to be replaced during the time of our CFHT observations and no simultaneous photometric coverage was obtained. Nevertheless, our database now consists of a total of 1588 VI_C data points, each having the mean of three readings of variable minus comparison (Figure 1). All measurements were made differentially with respect to HD 27159 as the comparison star and HD 76549 as the check star. Integration times were 30 s in V and I_C, respectively. For details on the robotic observing procedure and the automated data reduction, we refer the reader to Granzer et al. (2001).

The photometric observations from the University of Vienna APT are completely consistent with those of Grankin et al. (2008).

All spectroscopic and photometric data in this paper are phased with the photometric ephemeris of Stelzer et al. (2003),

$$\mathrm{HJD} = 2,452,234.285971 + 1.871970 \pm 0.000010 \times \mathrm{E}, \quad (1)$$

where the period has been obtained by minimizing the O–C residuals of the phases of the light curve minima between 1991 and 2001. This period represents the rotational cycle for the main spot group that dominated the observed light curve in the decade between 1991 and 2001. We have taken this to be the averaged surface rotation period of the star for the purposes of our analysis. In Section 3, we arrive at a comparable period from a periodogram analysis of the APT data in Figure 1.

2.3. The TempMap Code

To invert a phased sequence of observed spectral line profiles to obtain a temperature map of the surface, TempMap computes an error function that represents the degree to which the predicted spectrum from a current trial temperature image of a star (starting with a blank surface) differs from the observed spectrum. The error is expressed as the squared difference between the forward calculation and the observation summed over all wavelengths of the line profile on a point-by-point basis and over a full set of observations spaced in time through the full cycle of phases of the star's rotation. The program then alters the temperature pixels of the image to iteratively reduce the error function to a minimum consistent with the error of the observations. A regularizing functional of the minimization process—Tikhonov in this case—is used so that the line profiles calculated from the image produced do not overfit the observed spectra. For a full discussion of DI with TempMap and the process of regularization, see Rice (2002) and Piskunov & Rice (1993), and for parameter tests, see Rice & Strassmeier (2000).

In the current application, the local intensity line profiles were calculated from 12 Kurucz (1993) model atmospheres covering 3500 K to 6000 K of fixed $\log g$ of 4.0 for the purpose of recovering the local effective temperatures. These calculations were done assuming LTE and utilizing data from Kupka et al. (1999). Photometry was not included in the inversions, as it had been in earlier work on V410 Tau, because our APT data were not strictly simultaneous with the spectroscopy. An option in TempMap code is to use the program Spectrum (Gray 2000) for the calculation of local intensity line profiles. The option of using Spectrum was applied when TempMap was used on the TiO molecular band at 705.4 nm.

2.4. The iMAP Code

A new ZDI code iMAP was designed for the application to polarized spectral line profiles of late-type stars (Carroll et al. 2007; Kopf et al. 2009). The code uses a new multi-line cross-correlation technique by means of a PCA to extract and enhance the quality of individual (polarized) line profiles. It implements the full (polarized) radiative transfer equation and uses an inversion strategy that can incorporate prior knowledge, e.g., limit the maximum field strength to the equipartition

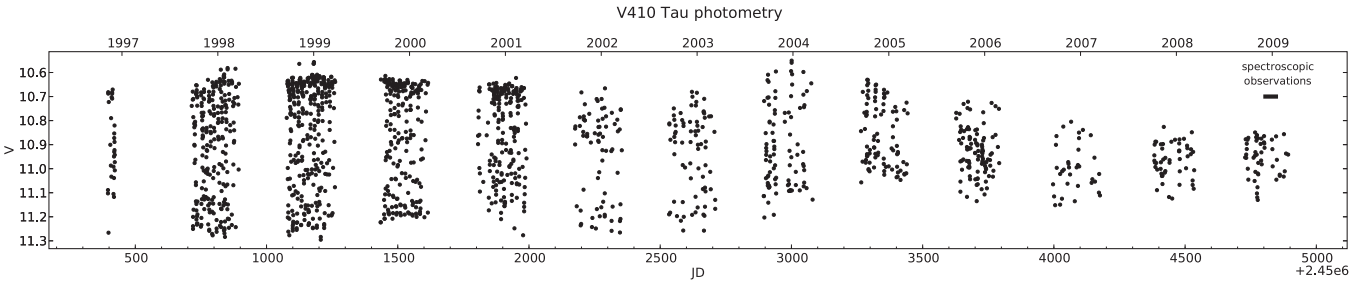

Figure 1. Long-term APT photometry of V410 Tau. Only the *V* data are shown. The data from which this figure is prepared are available electronically with a sample layout shown in the Appendix as Table 1. Note that the spectroscopic observations of this paper were obtained during the most recent observing season in 2008 December and 2009 January which appeared to be also the one with the smallest photometric amplitude ever observed for V410 Tau.

field strength as a function of line-formation depth, based on similar solar calculations. Moreover, the code utilizes a new regularization scheme which is based on local maximum entropy to allow a more appropriate reproduction of complex surface fields as would be expected for late-type stars (see Carroll et al. 2009). Standard applications of maximum entropy, or Tikhonov functionals, are applied globally and minimize the information content across the entire stellar disk, while local maximum entropy minimizes the information content locally wherever there is a signal, e.g., on or around the stellar rotational pole. The current application to V410 Tau was done without using this mode because only Stokes-I spectra were analyzed.

iMAP minimizes a discrepancy function of the form $E = 1/(n-1)\sum(O-C)^2$ by adjusting the free surface parameters. Here, n is the total number of wavelength points in all rotation phases. The free parameters are temperature and the three-component magnetic field, assigned to each surface segment. In the current application, iMAP was used in Stokes-I mode, so only the temperature was inverted. While the inversion is performed on the basis of a $6^\circ \times 6^\circ$ surface grid, the radiative transfer calculation is done on a $2^\circ \times 2^\circ$ grid. This allows for a precise line-profile synthesis while keeping the number of free parameters at a computationally reasonable value. With the $6^\circ \times 6^\circ$ grid there are 1800 surface elements. The minimization of the discrepancy function is carried out by a conjugate gradient method.

The PCA de-noising method uses a large number of spectral lines to decompose them into their eigenspectra. By using only the most significant eigenspectra to reproduce individual spectral line profiles, those with largest eigenvalues, the noise can be partly eliminated. To generate a list of spectral lines which are utilized for this analysis, we synthesized local line profiles of all lines listed in the Vienna atomic line database (Kupka et al. 1999) between 480 nm and 850 nm. Only those were selected which had a line depth larger than 0.6. The synthesis was based on a Kurucz ATLAS-9 atmosphere with the stellar parameters of V410 Tau. The number of spectral lines finally selected was 747.

3. ATOMIC LINE DOPPLER IMAGING WITH TWO DIFFERENT CODES

3.1. Adopted Stellar Parameters for V410 Tau

For this paper, we adopt the same set of relevant stellar parameters as summarized in Rice & Strassmeier (1996), but just re-optimized the $v \sin i$ and i parameter combination with the present data set (Figure 2). In particular, we fix our DI input to a logarithmic gravity of 4.0, an initial trial photospheric temperature of 4400 K, a $v \sin i$ of 77.7 ± 0.5 km s^{-1} at an

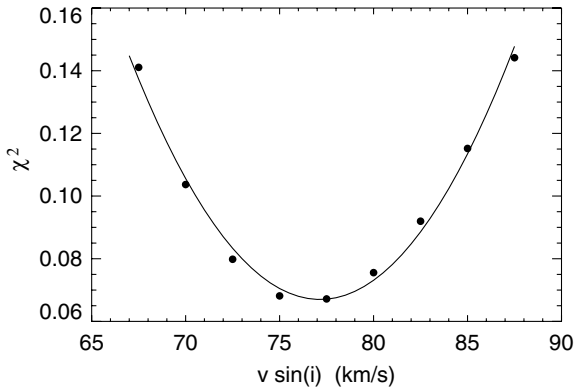

Figure 2. Optimization of the projected rotational velocity and inclination of the rotational axis for V410 Tau. Our best values are $v \sin i = 77.7$ km s^{-1} and $i = 62^\circ$ for the de-noised Fe I 549.5 nm line.

inclination of $i = 62^\circ \pm 2^\circ$, micro and macroturbulences of 2.0 km s^{-1} and 1.5 km s^{-1}, respectively, and standard solar chemical abundances.

Stelzer et al. (2003) had revised the ephemeris from a combination of literature data with some of the data presented later by Grankin et al. (2008). Their new photometric period was derived by aligning the minima of the phase-folded light curves for each observing season to coincide with phase zero. The difference from the period from Petrov et al. (1994) was 0.000125 days or $\Delta P/P \approx 6 \times 10^{-5}$. Such a small difference is not important for individual Doppler images but is important for the determination of the photometric minimum over long time intervals. However, such a period is model dependent and also depends on a hypothetical mechanism that produces spots in a way that the photometric minimum always appears at the same longitude.

For comparison, we use our own photometric time series from 1996 to 2009 (Figure 1) to obtain an independent value for the photometric period directly from the data. We employed five different period-search techniques (cf. Kolláth 1990) for the full data set, spanning 13 years between 1996 and 2009. The results were unambiguous and in excellent agreement with each other. A period of 1.871950 days was found with a discrete Fourier transform followed by a nonlinear optimization of its peak, 1.871950 days were obtained with the CLEAN algorithm and a Gaussian fit to its peak, 1.87194 days with a Lafler–Kinman algorithm and a Gaussian fit, 1.871953 days with the minimum string-length method and a Gaussian fit, and 1.871949 days with the phase-dispersion method and a Gaussian fit. Typical error bars are ±0.00001 days for each method. Therefore, our average value of 1.871948 days is very precise (rms of 4 ppm) and agrees within the errors with the independent value obtained by Stelzer

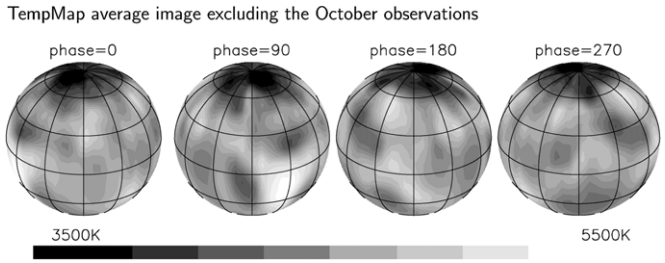

Figure 3. Averaged orthographic temperature map from Stokes I with TempMap. The map is an unweighted average from the eight lines mentioned in the text but using only the observations taken in 2008 December and 2009 January.

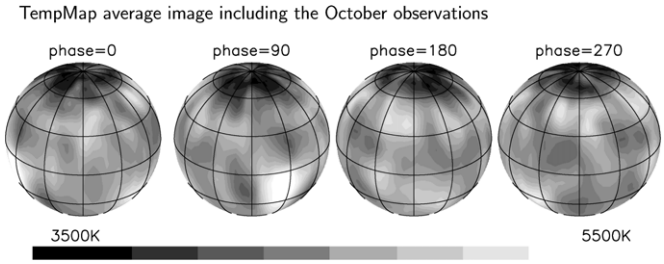

Figure 4. Averaged orthographic temperature image from Stokes I with TempMap. The image is an unweighted average from the eight lines mentioned in the text but using all observations including those taken in 2008 October.

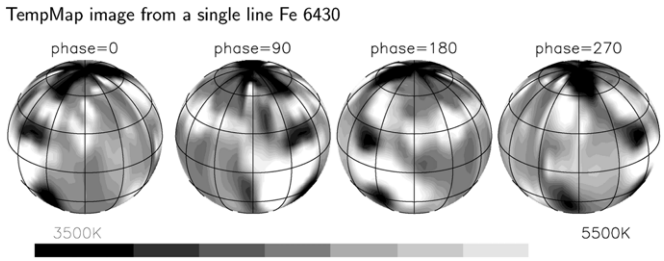

Figure 5. Orthographic temperature map from Stokes I with TempMap. This image is based on only the data from the Fe I 643.0 line which is one of the eight lines listed in the text as used in forming the multi-line average image. Only the observations of 2008 December and 2009 January were used for this image.

et al. (2003). This verifies that the coherent phase alignment of the photometric minimum of V410 Tau is indeed real. For consistency reasons, we adopt the ephemeris from Stelzer et al. (2003) as given earlier by Expression (1).

3.2. Multi-line Inversion with TempMap

We first proceeded with a line-by-line inversion using eight atomic lines. Our major lines were Fe I 639.3 nm, Fe I+Fe I 640.0 nm, Fe I 641.1 nm, Fe I 643.1 nm, Ca I 643.9 nm, Ni I 664.4 nm, Fe I 667.8 nm and Ca I 671.8 nm. Plots of wavelength ranges covering these lines were shown in our previous paper (Rice & Strassmeier 1996). Doppler images were obtained for each line using first only the 13 observations obtained in 2008 December and 2009 January. All 13 observations from this period were used except for those of the line Fe I 667.8 nm where the red wing of the line seemed very significantly distorted at phase 0.1809. This was the phase when a large flare occurred on V410 Tau as described in Section 5 of this paper. There is no evident reason why one would expect an Fe line with no blended feature of significance to be flare sensitive and to show such distortion, so it may just be an observational anomaly that the line was apparently affected. In any event, the effect was so significant that the phase was excluded from the observations of that line. Doppler images were also generated using all 17 observations including the four from 2008 October except for the anomalous phase for the 667.8 nm line as before. Initially, we showed concern at the number of stellar rotations that were involved in the time span from October through January and so we were reluctant to consider images generated including the October data. Given the very small differential rotation of V410 Tau and the consistency of the image of V410 Tau shown over 13 months in our earlier paper (Rice & Strassmeier 1996), we decided to use both the data set with the October observations and the data set without the October observations to see if adding the October data significantly degraded the image.

With TempMap, the atomic line data for each line feature used for generating images are taken from the VALD database (Kupka et al. 1999). TempMap calculates the local line profiles used for generating each image from the complete line blend represented in the observed feature using all significant adjacent lines from the VALD list.

The fitting errors that we achieve for the individual lines and line blends are comparable, e.g., 7.9×10^{-3} for the Fe I 643.1 nm line corresponding to an S/N ratio of 126:1. The ideal fit would be achieved for an S/N ratio that matches the observed one, i.e., on average 160:1. The error is defined here as $\sqrt{\sum (O-C)^2/(n-1)}$, where n is the number of spectrum points in all of the observations, i.e., the number of spectrum pixels per phase times the number of phases. This number of data points is such that the problem is essentially overdetermined and the least-squares fit predominates. We have two to three times as many profile points per star image in total as we have image pixels (2592) visible on the surface of each star.

Our final pixel-by-pixel averaged temperature images using TempMap based on the Doppler images from the eight lines listed above are shown in Figure 3 and Figure 4. The average image shown in Figure 3 is that developed from the 13 observations without 2008 October and the image of Figure 4 is from all 17 observed phases including October. It is evident that there is little difference between these two images. As a sample of an image from a single line, the image developed from the Fe I 643.1 nm line is shown in Figure 5. The theoretical line profiles calculated from that image along with the observations of Fe I 643.1 nm are presented in Figure 6.

3.3. De-noised Single-line Inversions with iMAP

A total of 747 spectral lines in the range 480–850 nm were used to de-noise time series of four particular spectral lines; Fe I 549.7516 nm (excitation energy of 1.011 eV, $\log(gf) = -2.849$), Fe I 641.1649 nm (3.654 eV, $\log(gf) = -0.595$), Fe I 643.0846 nm (2.176 eV, $\log(gf) = -2.006$), and Ca I 643.9075 nm (2.526 eV, $\log(gf) = 0.470$). The basic free parameter of the PCA de-noising method is the number of its principal components. No strict rule can be given for the choice of this value, but we follow the strategy laid out in Martínez González et al. (2008). This procedure suggests two components for our Stokes-V data and 12 components for the Stokes-I data.

The temperature images of V410 Tau obtained from the individual lines are shown in Figure 7 and the average map from all the four lines is shown in Figure 8. Figure 9 shows the fits to the de-noised line profiles on a line-by-line basis using iMAP. The fitting error is defined in iMAP as $E = \frac{1}{(n-1)} \sum_\phi \sum_\lambda (O-C)^2$, where $\phi = 1, \ldots, 12$ is the number of phases and $\lambda = 1, \ldots, m$ is the number of pixels per line

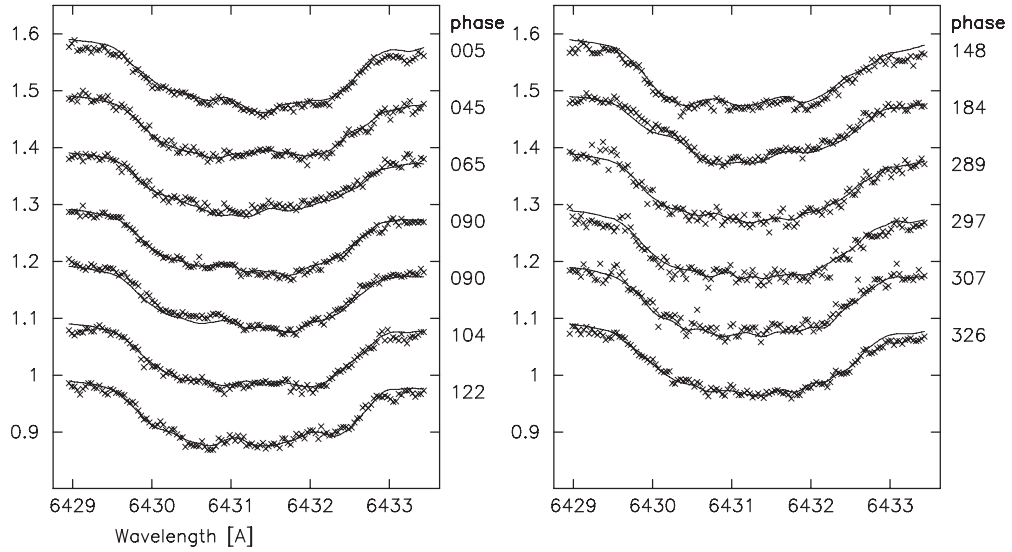

Figure 6. Fit to the profile at each phase of the line Fe I 643.1 nm in making an image from a single spectrum line using TempMap.

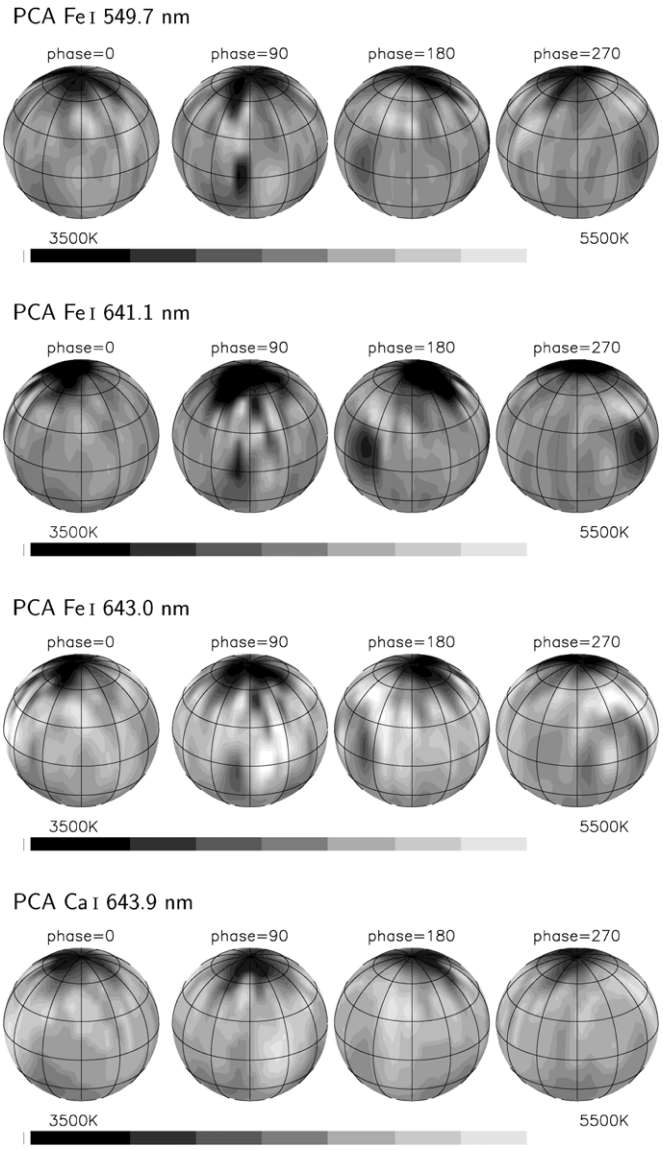

Figure 7. Orthographic temperature maps from Stokes I with iMAP.

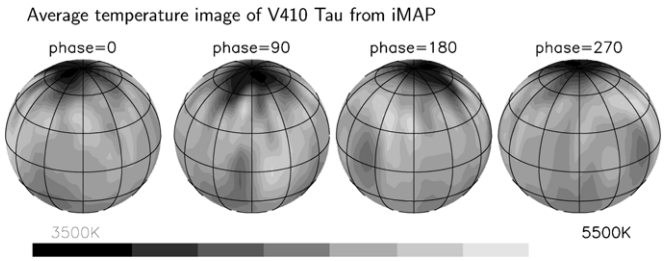

Figure 8. Average orthographic temperature map of V410 Tau obtained from four Stokes-I profiles with iMAP.

profile used for the inversion ($m = 241$ for Fe I 549.7, $m = 301$ for the other lines). The total number of available data points is $n = 12 \times m$. The following fitting errors were achieved: 2.9×10^{-5} for Fe I 549.7, 2.9×10^{-5} for Ca I 643.9, 3.0×10^{-5} for Fe I 641.1, and 3.9×10^{-5} for Fe I 643.0. This corresponds to S/N ratios between 160:1 and 185:1, comparable with the S/N of the original data. Although significantly better than with TempMap, it is still far away from the 1100:1 ratio of the de-noised input data. This indicates that most of the remaining noise is not photon noise but of external origin, mostly related to continuum placement errors, as already discussed and emphasized in Rice & Strassmeier (2000).

3.4. Comparing TempMap and iMAP Image from the Atomic Lines

Rice & Strassmeier (2000) do extensive tests on the ability of the DI process to recover the features in a spectrum calculated from an artificial test star surface containing features that one might expect to find on an actual active cool star: features such as the polar cap, high-latitude cool spots and equatorial cool spot features, spots with a small umbra and penumbral-like structure, and hot spots. The recoveries were done under varying conditions with varying axial inclinations, periods (equatorial velocities) and with varying S/N in the spectrum, and with artificially introduced external errors such as misplaced continuum and undetected blends or errors in line data. The recoveries were done with TempMap using the standard computational grid of 5° squares on the surface of the star. In general, for a star with the S/N of the spectra used here for

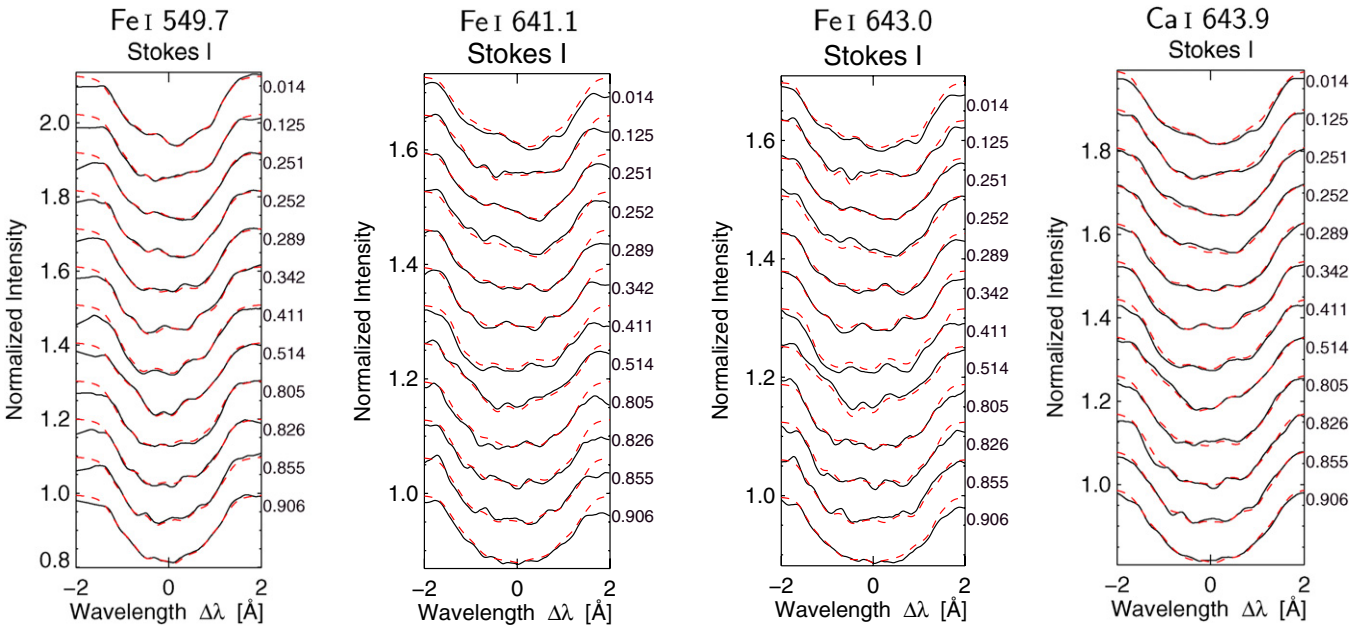

Figure 9. Stokes-I line-profile fits with iMAP. The full lines are the observations, the dashed lines are the fits.
(A color version of this figure is available in the online journal.)

V410 Tau and for a star with the period of V410 Tau, the recovery would have the following characteristics. The resolution on the surface would be better than 10° squares and in the case of the small features with small umbra-like centers of less than about 7°, the recovery did not recover the umbra, and the average temperature for the whole feature was very close to the temperature of the much larger penumbra. The accuracy of recovery in shape, position, and temperature was best at higher latitudes, and at more equatorial latitudes the near redundancy of behavior for features just north and south of the equator produced a tendency for the features there to be extended in latitude. Those features did not maintain a better than 10° accuracy in reproducing shape in the latitude direction and the temperature reconstruction was correspondingly reduced, depending on the stretching of the feature. The major errors in the image in the form of the temperature and location of spots came from the external errors rather than photon noise and because of that the best determinant of reliability comes in the form of multiple images from independent lines in the spectrum and if possible from sets of independent observations. The features the independent images have in common are those least likely to have been introduced through external error sources.

A comparison of the TempMap image of V410 Tau (Figure 3) based on observations from eight atomic lines that excluded the October data and the image of V410 Tau from iMAP (Figure 8) based on the same time period but using four de-noised atomic lines (one different than used by TempMap) shows very similar features. The polar cool cap is similar in the projections to lower latitudes. There are slight adjustments in latitude for some of the cool spots near the equator, but the spots are generally in close proximity. An exception is a cool spot seen at latitude near +20° and longitude 60° (i.e., subsolar at phase 60°) in the TempMap image that is absent in the iMAP image. The iMAP images completely excluded the flare-affected data from phase 0.1809 (65°), whereas only the anomalous profiles of one line were excluded from the TempMap input data and this is the likely source of this deviation. The hot feature just south of the location of this spot and slightly below the equator and seen in both images but somewhat stronger in the TempMap image is the likely source of the flaring activity reported later in this paper.

In summary, the major consistent features between these two images are as follows. There is a large and strong polar feature that is symmetric about the pole with an irregular boundary having short projections to lower latitudes such as the ones at longitudes of 110° and 240°. The temperature throughout this region is fairly consistently between 700° and 750° below the average photosphere temperature. At lower, more equatorial latitudes are a number of cool spots such as those just below the equator at longitudes of 90° and 135° and another at a latitude of 25° north and a longitude of 225°. Less reliable are the large irregular cool areas near the limits of visibility in the south. All of these cool spots have a temperature about 450° below the photospheric temperature. There are a few hot spots with the largest being at a longitude of 60°–65° and a latitude of the equator and below. The temperature of this feature in the model is at approximately 1000° above the mean photospheric temperature.

The cool spots at more equatorial latitudes and at temperatures of 450° below photospheric may, given the results of Rice & Strassmeier (2000) and bearing in mind the grid resolution of 5°, represent just the outline of features that have a much cooler small umbra. The temperature would represent the temperature of the penumbra as shown by similar test features in Rice & Strassmeier (2000). For the polar feature at the much lower temperature, it is much harder to conjecture as to the detail that might be hidden in the features since there is no comparable solar feature to guide our thinking. As for the large hot feature, there may be structure inside the boundaries such as is seen with faculae on the Sun but again, bearing in mind the grid size, the detail would not be apparent in the model.

4. MOLECULAR-LINE DOPPLER IMAGING WITH TempMap

As mentioned earlier, TempMap has a code option to use calculations of segments of intensity spectrum at different

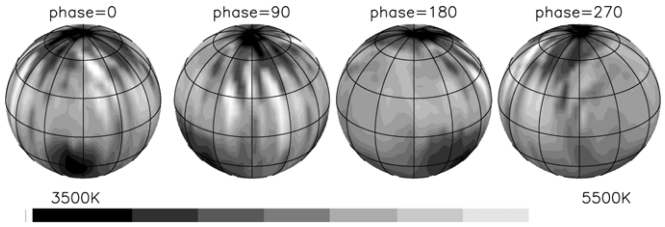

Figure 10. Averaged orthographic temperature map for V410 Tau produced from the TiO band at 705.4 nm. Only the observations of 2008 December and 2009 January were used for this image.

atmospheric effective temperatures and surface line-of-sight from the Spectrum code by Gray (2000) for the local line profiles. This allows the use of Spectrum to calculate the local line profiles necessary for inverting molecular bands in the spectrum of a star for images generated from spectral elements that are much stronger in the cool spot features of stars. Molecular-line integration for the local line profiles is not contained in the basic TempMap code, and it is in the Spectrum code, so this option is necessary for using TempMap when working with the molecular lines. The two line integration codes give the same results for atomic line calculation, so it is far easier to simply calculate local line profiles for the atomic lines internally in TempMap.

Because the molecular lines are much stronger in the cooler features of active stars, the idea of using molecular lines for Doppler images is something that has been thought about often in the past but the downside of using molecular bands for Doppler images is that the details of surface images are most strongly defined by the varying behavior of the wing components of lines. This is particularly true for defining the latitude of features on the star image. In molecular bands these wing variations are swamped by the blending together of adjacent, tightly packed molecular lines so the images are at best crude representations of the surface detail. Even though the expected result was a crude image, we tried a reconstruction from the TiO 705.4 nm band of V410 Tau to see if, at least, we would learn more about the actual temperature differential between the strong polar spots and the rest of the star. The reproduction of the temperature map of V410 Tau generated using the TiO band, admittedly poor in detail, is shown in Figure 10. This image was developed using a maximum entropy penalty function.

The molecular image is clearly different in detail from the images generated from the atomic lines using both DI programs, both for the atomic line average image and the individual atomic line images that are quite consistent among themselves. Only in a superficial way do we see some resemblance between the TiO image and atomic line average images in the features at equatorial latitudes. The polar cool spot is less concentrated at the pole and more distributed in a ragged pattern at somewhat lower latitudes. The hot spot seen in the atomic line images near longitude 60° (i.e., subsolar at phase 60°) is apparently stretched out (i.e., poorly resolved) in latitude and ragged like the polar feature. This is not an unexpected result given the comments made above. In particular, the lack of good information from the line wings would affect the equatorial regions more strongly than the polar regions. An additional complication is the problem of clearly establishing the continuum level throughout the TiO band region, a complication that, again, would strongly influence the equatorial regions and normally make the average global temperatures unreliable. Indeed, the average effective temperature over the whole visible surface of the star in the TempMap atomic line images at approximately 4450 K–4500 K is about 100° hotter than the average for the image formed from the TiO molecular feature, so the problems present in establishing the continuum for the TiO band may be expressed in this difference. The average temperature right near the pole at the center of the large cool polar region differs by about 150° from the atomic line image such that the atomic line image displays an average effective temperature there of about 3750°, and the TiO image suggests that the average polar temperature is just under 3600°. This is likely part of the overall lower temperatures in the TiO image. It is also possible that this is influenced by the poorer resolution for the TiO image. Alternatively, the molecular lines of TiO might give a more accurate representation of the differences in temperature in the cool spots compared to the rest of the photosphere, since they are so much stronger and more sensitive to temperature in the cool regions.

The two strong cool features seen in the molecular map near the limit of visibility in the south at phases 0° and 180° (near longitude 150°) are not explained and are presumably due to the poor resolving capacity with the TiO feature and to the fact that the least information for DI is available for the regions below the equator at the limit of visibility.

A future attempt to reconstruct with molecular features might be tried with a much more slowly rotating star where the densely packed molecular components would be closer to resolved. In a more slowly rotating star, the wing components would be less obliterated and the continuum more reliable.

5. DISCUSSION

5.1. Inventory of Previous Doppler Images of V410 Tau

Our own first Doppler image of V410 Tau was based on KPNO–PennState echelle spectra at a resolving power of 12,000 and S/N of 120–150 and was taken in 1992 (Strassmeier et al. 1994). Independently, Joncour et al. (1994) obtained an image based on observations at the Observatoire de Haute Provence at a resolution of 32,000 and S/N of 50–115 taken in 1990. One year later, in 1993 December, Rice & Strassmeier (1996) employed the much larger CFHT and its coudé spectrograph at a resolution of 27,000 and S/N of 200:1 and compared this new map with the maps obtained one year earlier. From that they concluded that the differential rotation $\Delta\Omega/\Omega$ on its surface must be very small, approximately 100 times smaller than on the Sun. Coincidentally, Hatzes (1995) observed V410 Tau simultaneously with our CFHT observations in 1993/1994 at the McDonald Observatory at a resolution of 40,000 and S/N of ≈160. Rice (2002) compared these two images in his review at the first Potsdam ThinkShop. His plot demonstrated the encouraging similar reconstructions despite the fact that the maps were from different telescope–spectrograph combinations, had different inclinations adopted for the inversion, were with and without photometry as additional input, and that the inversions were done with two independent, and markedly different, DI codes. Schmidt et al. (2005) used the 2 m Tautenburg telescope and its coudé spectrograph at a resolving power of 31,500 and S/N of ≈ 100 from 2004 November to 2005 March (presented in a masters thesis at the University of Jena). Most recently, Skelly et al. (2010) presented a brightness image from data taken with NARVAL at the 2 m Bernard Lyot telescope from 2009 January 2 to 2009 January 17 ($R = 60{,}000$ and S/N between 102:1 and 166:1). It also revealed a polar spot and groups of low-latitude spots fairly evenly distributed in longitude.

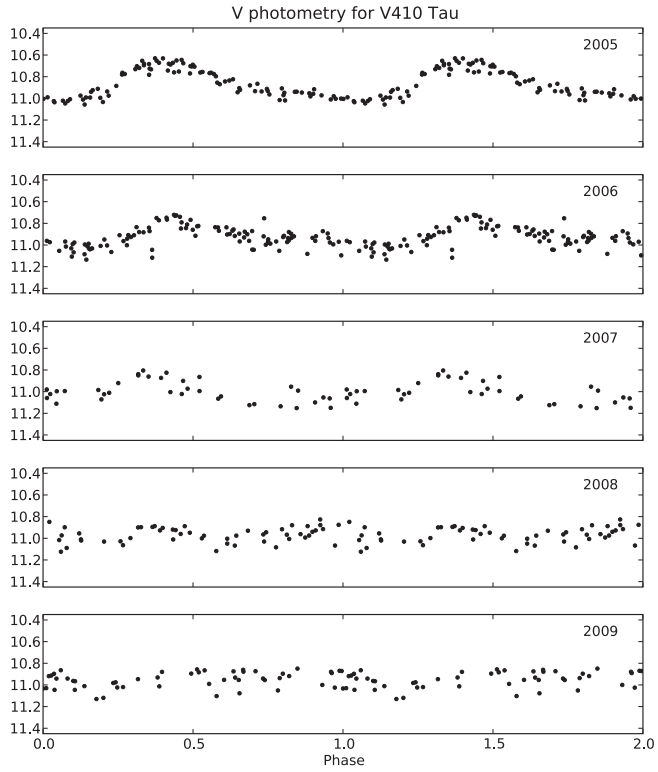

Figure 11. Phased light curves of V410 Tau for the observing seasons 2005–2009. For the first time after ≈ 20 years of continuous monitoring, V410 Tau entered a time of low-amplitude activity in 2008. Our DI from spectral line profiles agrees with such a low amplitude and even predicts a double-humped light and color curve for that time.

5.2. The Long-term Spot Evolution

Grankin et al. (2008) presented seasonal light curves from 1986 to 2004, i.e., for 19 consecutive years, and demonstrated the consistent phase alignment of the light curve minimum of V410 Tau. We verify this alignment with our new periodogram analysis of resolved rotationally modulated light curves (rather than seasonally averaged phase-folded light curves with posteriori O–C minimization). We also extend the time line for another five years and caught the star during a time of rather small photometric amplitude in 2008 and 2009. Also, the shape of the light curve and thus the spot distribution on the stellar surface changed over the years (cf. Figures 1 and 11) but never masked out the persistent phase alignment. A comparable behavior is seen for other spotted WTTSs, e.g., LkCa7, LKCa4, TAP41, and V830 Tau (Grankin et al. 2008), with some deviations, e.g., for V830 Tau, but never as pronounced as for V410 Tau. The interpretation for this behavior is straightforward as being due to an active longitude with variable amounts of activity. The question is why does V410 Tau not flip back and forth (flip-flop), as in some evolved spotted stars, singles, and binaries, and as explained via a non-axisymmetric mode instability of the dynamo? Flip-flop periods between 3 and 20 years are observed (Korhonen & Järvinen 2007). We may speculate that such a flip-flop on a T Tauri star has a much longer timescale, possibly aperiodic, and that we have just the beginning of a flip in 2008. Clearly, continuing time series monitoring with high cadence is needed to be more firm.

5.3. Doppler Image Comparison, 1993 and 2008

Figure 12 compares the Doppler image obtained from observations taken in 1993 December with the current temperature

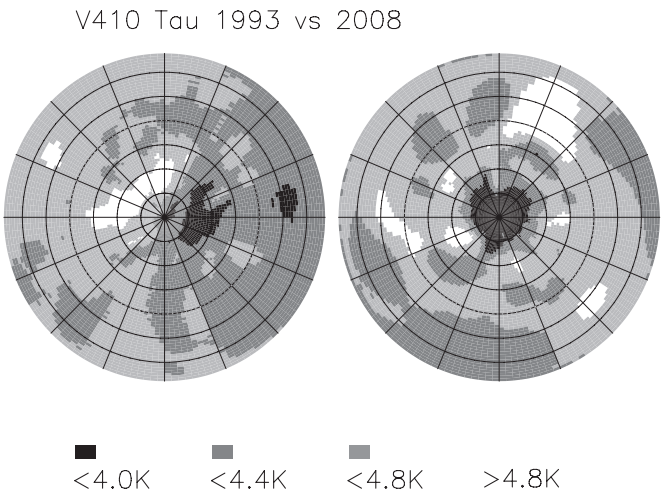

Figure 12. Polar depiction of the changes in the spot pattern for V410 Tau as seen in 1993 (Rice & Strassmeier 1996; Rice 2002) compared to the 2008 December image presented here. The dramatic large-scale cool hemisphere of 1993 explains the extreme photometric variability at that time and the more uniform distribution of cool features in the 2008 image clearly produces much less variability. Note that the image for 2008 has longitude zero extending to the right from the pole and longitude 90° is up. The coordinates of the 1993 image are based on the ephemeris used in the papers cited above.

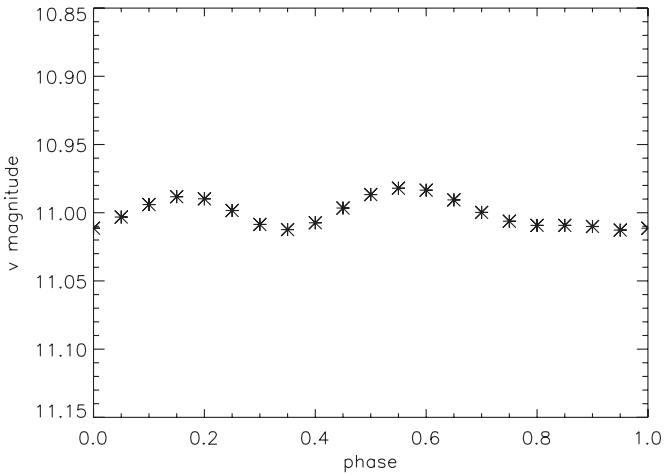

Figure 13. Prediction of the apparent v photometric variation for 2008 December based on the V410 Tau average temperature map is shown in Figure 3. The vertical axis is the calculated v magnitude in steps of 0.01 magnitudes and the horizontal axis is the phase. The full amplitude of variation is 0.03 magnitudes

image determined from observations in 2008 December to 2009 January. The 1993 image was constrained by simultaneous photometry and the source of the extreme variation in apparent V magnitude for V410 Tau in the mid-1990s is clear. The star is much cooler in the entire hemisphere visible near phase 0 and there is a high-latitude, large, very cool spot at the phase 0 longitude. The variability in V at that time (see Figure 1) approached 0.6 mag. The right-hand image in Figure 12, while not constrained by simultaneous photometry, clearly shows that the temperature distribution in longitude is much more uniform in 2008 and the high-latitude feature is now a polar feature and so not in a position to contribute to photometric variability to any degree. A calculation of the V light curve that would be produced as a result of rotation with this surface temperature distribution is given in Figure 13 and shows, as would be expected from the image, a virtually constant V magnitude. Figure 12 portrays the surface changes on V410 Tau that have resulted in the virtual disappearance of the V variability quite vividly.

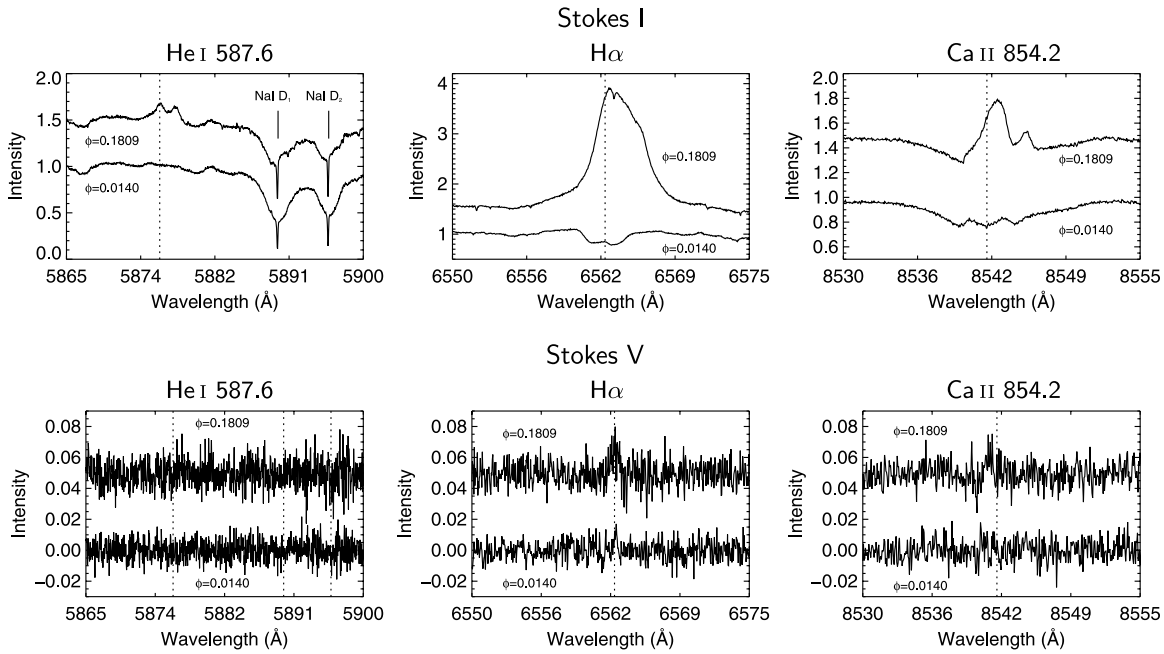

Figure 14. Examples of flare-affected spectral regions. The top panels show Stokes-I spectra of He I 587.6, Hα, and Ca II 854.2 (from left to right). The bottom panels show Stokes V. Each panel compares a flare spectrum, shown as the top spectrum (shifted arbitrarily by 0.5 in intensity), with a "quiescent" spectrum below. The vertical dotted lines indicate the laboratory wavelengths. A Stokes-V signal is detected for Hα and the Ca II IRT, but not for He I.

5.4. Hot Spots

Hot spots, such as those shown in our current 2008 temperature map of V410 Tau and the two maps published earlier (Rice & Strassmeier 1996; Strassmeier et al. 1994) as well as in Skelly et al. (2008) and Strassmeier et al. (2005), have been discussed in these earlier publications from the point of view of their reality and possible underlying cause. In Rice & Strassmeier (1996), we examined the presence of the hot spot visible in the left image of Figure 12 formed by both weak and strong lines and found the spot to be consistently there in all images. Strassmeier et al. (2005) were able to connect the location of a similar hot feature on MN Lup, through Balmer line emission, to the likely location of an accretion shock from material funneling down from residual circumstellar material surrounding that transitional WTTS star. It appears unlikely that accretion from a circumstellar disk can explain the hot spot in V410 Tau, as was pointed out in Rice & Strassmeier (1996), but the possibility of a facular-type explanation was mentioned. In support of this idea, we might note that Skelly et al. (2008) analyzed the Balmer lines in the spectrum of the WTTS TWA 6, and he was led to propose the existence in the chromosphere of active regions associated with the spot features of that star that were similar to solar plages.

5.5. A Large Flare During the DI Observations

V410 Tau is also known to exhibit the most energetic flares known among T Tauri stars ($>10^{37}$ erg; see the compilation in Fernández et al. 2004). Our DI time series observations caught V410 Tau during a large flare event on HJD 2,454,816.07124 (phase 0.1809).

Figure 14 compares three spectral regions during the flare event (phase 0.1809) and the "quiescent" state (phase 0.0140) for both Stokes I and V. All flare emission lines appear redshifted with respect to the non-flaring wavelength. The Hα central emission is redshifted by approximately 59 ± 7 km s^{-1}, but this remains difficult to measure due to the asymmetric line shape. Note that the total width at continuum level increased to $\approx$660 km s^{-1} (14.5 Å) during the flare, in agreement with the Hα flare modeled by Fernández et al. (2004). He I 587.6 nm emission is detected only during the time of the flare at a redshift of 52.5 ± 0.5 km s^{-1} and a full width at the continuum level of $\approx$255 km s^{-1}, and is not seen at any other phase. It appears with a strong central absorption reversal, commonly seen for cooled material on top of a hot ejecta.

Hα and possibly also the Ca II infrared triplet lines reveal a Stokes-V signal, while He I 587.6 or the sodium D lines clearly do not (see Figure 14). The Ca II H and K spectra show the same asymmetry in Stokes I but have not enough counts for a useful Stokes *V* spectrum. The magneto-sensitive Fe I 524.7 and 525.0 nm lines appear to be unaffected by the flare, both in Stokes I and V. The Stokes-V peak separation for the two lines is a typical indicator for flux-tube magnetic fields during solar flares (e.g., Kostenko & Lozitskij 1996).

The Doppler images from photospheric atomic absorption lines indicate a single equatorial warm spot at $\ell \approx 60^\circ$ just below the equator, i.e., phase 0.17, almost coincidental with the phase of the flare peak as seen by the appearance of the strong Balmer emission lines (Hα, Hβ, Hγ, Hδ, and Hϵ). This is suggestive that there is a spatial relation between the flare site and this warm spot, which is more likely a huge active region.

A second, smaller double warm spot is reconstructed from our line profiles at $\ell \approx 210^\circ$, i.e., phase ≈ 0.58, and also coincides with another increase of Hα emission seen at phase 0.5957. For this event, however, the Hα emission appears blueshifted with respect to the laboratory wavelength by ≈ 160 km s^{-1}. We note that the latter spectrum was taken five nights after the flare peak, i.e., 2.42 rotation phases apart from the bigger flare. Therefore, it cannot be from the same event and is likely yet another flare that was not caught during its peak phase (we obtained at most one spectrum per night).

Comparable Hα flares were detected on other RS CVn stars, e.g., on the active subgiant HD 291095 = V1355 Ori (Strassmeier 2000). Its flare released 5×10^{34} erg in Hα and

was recorded when its huge and asymmetric polar spot crossed the central meridian, suggesting a near polar origin because that star showed mostly high-latitude photospheric activity.

6. SUMMARY

In summary, we have the following results:

1. The dramatic steady reduction in the amplitude of the photometric variation in the light curve for V410 Tau from the time of our Doppler images of 1992 and 1993 until 2008 might have been assumed to be a consequence of a reduction of spot numbers and total active surface area in the absence of the images contained in this paper. The observations presented here make clear that the reduction in photometric variability arises, instead, from a transition to a more axisymmetric distribution of spots from the highly asymmetric distribution of 1992 and 1993. The high-latitude strong polar spot at longitude roughly 0° in the earlier images is now apparent as a rather symmetric polar cap with average temperature throughout the cap of about 700°–750° below the photospheric temperature. Limited spatial resolution prevents any observation of detail in the temperature distribution within the cap better than the equivalent of 7° of latitude. The previously observed discrete features at more equatorial latitudes with temperatures between 400° and 500° below photospheric were located almost exclusively around longitudes from 270° through 0° to 90°. This could be described as a preferred longitude of 0° in the 1992 and 1993 images. These features, in 2008, are more uniformly distributed about all longitudes. The phenomenon of a preferred longitude appears to have disappeared currently. The same limitation on spatial resolution as was described for the polar cap applies to the more equatorial features, so these spots may contain much cooler, smaller "umbra-" like cores with the temperature of the whole feature rendered in the images as closer to the "penumbral" part of the spot feature.
   The flip-flop phenomenon is a reversal by 180° of longitude in the preferred longitudes for active regions on some cool stars as described earlier. Where observed, this reversal has had a quasi-periodic character. Our Doppler images of V410 Tau over the period from 1992/1993 to 2008 could represent just a redistribution of spots from some accidental collection around longitude 0° to a more random distribution around all longitudes. Given the known flip-flop behavior of other stars, though, it is more likely that we are seeing the beginning of a flip for V410 Tau from a preferred longitude of 0° to perhaps a preferred longitude of 180°. In any event, the very large reduction in photometric amplitude from 1993 to 2008 is not accompanied by a large reduction in the total area of spot activity.
2. Two hot regions in the Doppler image appear to be coincident with the location of separate flares that were revealed through emission in the Balmer lines, and in the He I and in Ca II lines. These hot regions are most likely similar to plage-like regions
3. The Doppler images through inversion of atomic lines using TempMap and a newer code iMAP produce gratifyingly consistent results with one another and from line to line in the sense that the polar feature is rendered in the same manner in both sets of images and the scattered cool and hot features throughout the lower latitudes are located in similar spots.
4. An experiment in inverting the TiO molecular feature at 705.4 nm shows that we obtaine good agreement of the surface temperature scale but that it is difficult to get a reliable, well resolved image from molecular features, especially with stars of large $v \sin i$, because of the overlapping of the wings in adjacent molecular lines in the band. Such overlapping in the wings obscures information necessary in DI for reconstructing features in the latitudes of the equatorial region.

J.B.R. acknowledges support from the Natural Science and Engineering Research Council of Canada (NSERC). K.G.S. is grateful to the German Science Foundation (DFG) for support under grant STR645/1. We thank Nadine Manset and the other CFHT staff for their continuous support. We thank also Thorsten Carroll for helping out with the iMAP computations.

Facilities: CFHT.

APPENDIX

APPENDIX MATERIAL

Table 1 lists the photometry of V410 Tau used to prepare Figure 1.

Table 1
Photometry of V410 Tau Used in Preparing Figure 1

HJD	Differential *V* Magnitude	RMS of Diff. *V* Magnitude
2450395.74781	+2.63270	0.00170
2450395.78937	+2.61880	0.00080
2450396.79379	+2.21190	0.00300
2450396.84406	+2.21770	0.00460
2450397.84084	+2.79620	0.03550
2450398.82439	+2.25280	0.00570
2450404.77296	+2.43060	0.00080

(This table is available in its entirety in a machine-readable form in the online journal. A portion is shown here for guidance regarding its form and content.)

REFERENCES

Aarum Ulvas, V., & Engvold, O. 2003, A&A, 399, L11
Alapini, A., & Aigrain, S. 2009, MNRAS, 397, 1591
Berdyugina, S. V. 2005, Living Rev. Sol. Phys., 2, 8
Berdyugina, S. V., Pelt, J., & Tuominen, I. 2002, A&A, 394, 505
Carroll, T. A., Kopf, M., Ilyin, I., & Strassmeier, K. G. 2007, Astron. Nachr., 328, 1043
Carroll, T. A., Kopf, M., Strassmeier, K. G., & Ilyin, I. 2009, in IAU Symp. 259, Cosmic Magnetic Fields: From Planets to Stars and Galaxies, ed. K. G. Strassmeier, A. G. Kosovichev, & J. E. Beckman (Cambridge: Cambridge Univ. Press), 633
Donati, J.-F., Catala, C., & Landstreet, J. 1998, in Proc. 5th CFHT Users Meeting, ed. P. Martin & S. Rucinski, 50
Donati, J.-F., Semel, M., Carter, B. D., Rees, D. E., & Collier Cameron, A. 1997, MNRAS, 291, 658
Elstner, D., & Korhonen, H. 2005, Astron. Nachr., 326, 278
Fernández, M., et al. 2004, A&A, 427, 263
Frasca, A., Kövári, Zs., Strassmeier, K. G., & Biazzo, K. 2008, A&A, 481, 229
Grankin, K. N., Bouvier, J., Herbst, W., & Melnikov, S. Yu. 2008, A&A, 479, 827
Granzer, T., Reegen, P., & Strassmeier, K. G. 2001, Astron. Nachr., 322, 325
Gray, R. O. 2000, SPECTRUM Program, Dept. of Physics and Astronomy, Appalachian State University, http://www.phys.appstate.edu/spectrum/spectrum.html
Hall, D. S. 1972, PASP, 84, 323
Hatzes, A. P. 1995, ApJ, 451, 784
Hatzes, A. P. 2002, Astron. Nachr., 323, 392
Herbst, W. 1989, AJ, 98, 2268
Järvinen, S. P., Berdyugina, S. V., & Strassmeier, K. G. 2005, A&A, 440, 735

Joncour, I., Bertout, C., & Ménard, F. 1994, A&A, 285, L25
Kitchatinov, L., & Rüdiger, G. 2005, Astron. Nachr., 326, 379
Kolláth, Z. 1990, The program Package MUFRAN, Occasional Technical Notes of Konkoly Observatory, 1 (http://www.konkoly.hu/Mitteilungen/Mitteilungen.html#TechNotes)
Kopf, M., Carroll, T. A., Ilyin, I., Strassmeier, K. G., & Tuominen, I. 2009, in ASP Conf. Ser. 405, Solar Polarization 5, ed. J. Stenflo, S. V. Berdyugina, K. N. Nagendra, & R. Ramelli (San Francisco, CA: ASP), 517
Korhonen, H., Berdyugina, S. V., Strassmeier, K. G., & Tuominen, I. 2001, A&A, 379, L30
Korhonen, H., & Järvinen, S. P. 2007, in IAU Symp. 240, Binary Stars as Critical Tools and Tests in Contemporary Astrophysics, ed. W.I. Hartkopf, E.F. Guinan, & P. Harmanec (Cambridge: Cambridge Univ. Press), 453
Kostenko, L. M., & Lozitskij, V. G. 1996, Astron. Nachr., 317, 259
Kupka, F., Piskunov, N. E., Ryabchikova, T. A., Stempels, H. C., & Weiss, W. W. 1999, A&AS, 138, 119
Kurucz, R. L. 1993, ATLAS-9, CD-ROM 13
Martínez González, M. J., Asensio Ramos, A., Carroll, T. A., Kopf, M., Ramírez Vélez, J. C., & Semel, M. 2008, A&A, 486, 637
Oláh, K. 2006, Ap&SS, 304, 145
Oláh, K., Strassmeier, K. G., & Granzer, T. 2002, Astron. Nachr., 323, 453
Petrov, P. P., Shcherbakov, V. A., Berdyugina, S. V., Shevchenko, V. S., Grankin, K. N., & Melnikov, S. Y. 1994, A&A, 107, 9
Piskunov, N. E., & Rice, J. B. 1993, PASP, 105, 1415
Rice, J. B. 2002, Astron. Nachr., 323, 220
Rice, J. B., & Strassmeier, K. G. 1996, A&A, 316, 164
Rice, J. B., & Strassmeier, K. G. 2000, A&A, 147, 151
Schmidt, T., Guenther, E., Hatzes, A. P., Ries, C., Hartmann, M., Ohlert, J. M., & Lehmann, H. 2005, Astron. Nachr., 326, 667
Skelly, M. B., Donati, J.-F., Bouvier, J., Grankin, K. N., Unruh, Y. C., Artemenko, S. A., & Petrov, P. 2010, MNRAS, 403, 159
Skelly, M. B., Unruh, Y. C., Cameron, A. Collier, Barnes, J. R., Donati, J.-F., Lawson, W. A., & Carter, B. D. 2008, MNRAS, 385, 708
Stelzer, B., et al. 2003, A&A, 411, 517
Strassmeier, K. G. 2000, A&A, 357, 608
Strassmeier, K. G. 2009, A&AR, 17, 251
Strassmeier, K. G., Boyd, L. J., Epand, D. H., & Granzer, T. 1997, PASP, 109, 697
Strassmeier, K. G., Rice, J. B., Ritter, A., Küker, M., Hussain, G. A. J., Hubrig, S., & Shobbrook, R. 2005, A&A, 440, 1105
Strassmeier, K. G., Welty, A. D., & Rice, J. B. 1994, A&A, 285, L17
Vrba, F. J., Herbst, W., & Booth, J. F. 1988, AJ, 96, 1032